HHS Public Access

Author manuscript

J Neurochem. Author manuscript; available in PMC 2023 May 03.

Published in final edited form as:

J Neurochem. 2023 May ; 165(3): 379–390. doi:10.1111/jnc.15793.

Lipid metabolism in dopaminergic neurons influences light entrainment

Regina F. Fernandez[1], **Emily S. Wilson**[1], **Victoria Diaz**[2], **Jonatan Martínez-Gardeazabal**[3], **Rachel Foguth**[4], **Jason R. Cannon**[4], **Shelley N. Jackson**[5], **Brian P. Hermann**[2], **Jeffrey B. Eells**[6], **Jessica M. Ellis**[1]

[1]Department of Physiology and East Carolina Diabetes and Obesity institute, Brody School of Medicine at East Carolina University, Greenville, North Carolina, USA

[2]Department of Neuroscience, Developmental and Regenerative Biology, University of Texas San Antonio, San Antonio, Texas, USA

[3]Department of Pharmacology, University of Basque Country, Leioa, Spain

[4]School of Health Sciences, Purdue University, West Lafayette, Indiana, USA

[5]National Institute on Drug Abuse, Intramural Research Program, Translational Analytical Core, Baltimore, Maryland, USA

[6]Department of Anatomy and Cell Biology, East Carolina University, Brody School of Medicine, Greenville, North Carolina, USA

Abstract

Dietary lipids, particularly omega-3 polyunsaturated fatty acids, are speculated to impact behaviors linked to the dopaminergic system, such as movement and control of circadian rhythms. However, the ability to draw a direct link between dopaminergic omega-3 fatty acid metabolism and behavioral outcomes has been limited to the use of diet-based approaches, which are confounded by systemic effects. Here, neuronal lipid metabolism was targeted in a diet-independent manner by manipulation of long-chain acyl-CoA synthetase 6 (ACSL6) expression. ACSL6 performs the initial reaction for cellular fatty acid metabolism and prefers the omega-3 polyunsaturated fatty acid, docosahexaenoic acid (DHA). The loss of Acsl6 in mice (*Acsl6*$^{-/-}$) depletes neuronal membranes of DHA content and results in phenotypes linked to dopaminergic control, such as hyperlocomotion, impaired short-term spatial memory, and imbalances in dopamine neurochemistry. To investigate the role of dopaminergic ACSL6 on these outcomes,

Correspondence Jessica M. Ellis, Department of Physiology and East Carolina Diabetes and Obesity Institute, Brody School of Medicine at East Carolina University, 115 Heart Drive, Greenville, NC 27834, USA. ellisje18@ecu.edu.

AUTHOR CONTRIBUTIONS

RFF, JBE, BPH, and JME conceived, designed, and interpreted data. RFF, ESW, VD, JMG, RF, JRC, and SHJ performed experiments and analyzed data. JME wrote the manuscript and obtained funding.

CONFLICT OF INTEREST STATEMENT

There are no conflicts of interest.

SUPPORTING INFORMATION

Additional supporting information can be found online in the Supporting Information section at the end of this article.

a dopaminergic neuron-specific ACSL6 knockout mouse was generated ($Acsl6^{DA-/-}$). $Acsl6^{DA-/-}$ mice demonstrated hyperlocomotion and imbalances in striatal dopamine neurochemistry. Circadian rhythms of both the $Acsl6^{-/-}$ and the $Acsl6^{DA-/-}$ mice were similar to control mice under basal conditions. However, upon light entrainment, a mimetic of jet lag, both the complete knockout of ACSL6 and the dopaminergic-neuron-specific loss of ACSL6 resulted in a longer recovery to entrainment compared to control mice. In conclusion, these data demonstrate that ACSL6 in dopaminergic neurons alters dopamine metabolism and regulation of light entrainment suggesting that DHA metabolism mediated by ACSL6 plays a role in dopamine neuron biology.

Keywords

acyl-CoA synthetase; docosahexaenoic acid; dopaminergic neurons; light entrainment; lipid metabolism

1 | INTRODUCTION

Neurons contain high levels of membrane phospholipids to support cell structure and neural activity (Manni et al., 2018). Neuronal phospholipids are enriched with the omega-3 polyunsaturated fatty acid, docosahexaenoic acid (DHA) (Crawford et al., 2013), a highly unsaturated fatty acid containing 22 carbons and six carbon–carbon double bonds termed unsaturation. One of the unsaturation points of DHA is found in the omega-3 location. Omega-3 double bonds cannot be synthesized by animals but are obtained from plant origins through the diet. The omega-3 fatty acid DHA has been implicated in numerous neuroprotective mechanisms affecting a range of neurological outcomes and disease processes, including those afflicting dopaminergic systems (Chitre et al., 2020; Guixà-González et al., 2016; Metz et al., 2019). Indeed, dietary DHA deficiency results in reduced levels of dopamine, dopamine receptors, and dopaminergic synaptic vesicles (Zimmer et al., 1998; Zimmer et al., 2002). Mechanistically, membrane DHA is shown to act as a high-affinity scaffold for dopaminergic receptors and to facilitate vesicle budding (Guixà-González et al., 2016; Manni et al., 2018). Together, these works suggest a role for DHA in dopaminergic-related neural activity.

We recently demonstrated that neuronal membrane DHA enrichment relies on the enzymatic activity of long-chain acyl-CoA synthetase 6 (ACSL6) (Fernandez et al., 2018, 2021; Fernandez & Ellis, 2020). ACSL6 is one of a large family of lipid-metabolizing acyl-CoA synthetase enzymes that activate fatty acids for metabolism within cells and influence the directionality of fatty acid metabolic flux (Ellis et al., 2010; Grevengoed et al., 2015; Marszalek et al., 2004). The deletion of ACSL6 in mice results in the depletion of neuronal membrane DHA content by ~50% (Fernandez et al., 2018, 2021; Fernandez & Ellis, 2020). ACSL6 knockout ($Acsl6^{-/-}$) mice demonstrate that hyperlocomotion behavior reflected by increased travel time, speed, and fewer freezing bouts observed across several distinct observational testing scenarios (Fernandez et al., 2018, 2021; Fernandez & Ellis, 2020). Dopamine is well established to regulate locomotion (Beninger, 1983), thus, herein, we questioned the role of ACSL6-regulated fatty acid metabolism in dopamine metabolism and dopaminergic control of motor activity and circadian rhythms (Partington et al., 2021).

We confirmed the expression of ACSL6 in dopaminergic neurons and showed that the germline deletion of ACSL6 resulted in reduced levels of membrane polyunsaturated fatty acids in brain regions enriched with dopaminergic innervations, along with altered striatal dopamine turnover. To assess ACSL6's specific role in dopaminergic neurons, ACSL6 was exclusively deleted in dopaminergic neurons using a Cre-floxed conditional knockout model driven by the dopamine transporter promoter ($Acsl6^{DA-/-}$). $Acsl6^{DA-/-}$ mice demonstrate reduced striatal dopamine turnover and hyperlocomotion. Using light-controlled housing, the challenge of a 6-h light entrainment to mimic jet lag led both $Acsl6^{-/-}$ and $Acsl6^{DA-/-}$ mice to exhibit maladaptive delays in recovery time. These data demonstrate that ACSL6 in dopaminergic neurons is critical for maintaining locomotor and circadian control.

2 | METHODS

2.1 | Mice

Acsl6 knockout mice were created using a vector designed by the NIH-sponsored knockout mouse program to target Acsl6 exon 2 and injected into C57BL/6 embryonic stem cells to generate Acsl6 conditional mice ($Acsl6^{flox/flox}$) by Ingenious Targeting, Inc, as described (Fernandez et al., 2018). $Acsl6^{flox/flox}$ mice generated were bred with either CMV-driven Cre to induce germline deletion, as previously described (Fernandez et al., 2018; Fernandez et al., 2021), or with dopamine transporter (DA)v specific Cre recombinase expressing mice (Strain #:020080, stock Slc6a3tm1(Cre)Xz/J from the Jackson Laboratory) to create mice with a deletion of ACSL6 specifically in dopaminergic neurons, $Acsl6^{DA-/-}$ mice. Mice expressing a 3x-Flag tag ligated to the C terminus of endogenous ACSL6 ($Acsl6^{Tag}$) were generated using small guiding RNA technology by the Animal Production & Gene Editing Core of Washington State University. Mice will be shared upon reasonable request per discretion of the investigator. All mice were housed in a 12-h light/dark cycle, unless housed in light-controlled chambers for circadian assessments, with ad libitum access to food and water. Tissues were collected after anesthetization with Avertin (2,2,2-Tribromoethanol, VWR cat. no. TCT1420) at 250 mg/kg body weight injected i.p. followed by decapitation. The use of Avertin was approved by the institutional board following East Carolina University DCM/IACUC Guidelines on the Use of Tribromoethanol (TBE), and the preparation and storage of the Avertin solution followed the manufacturer's instructions. Experiments performed with mice were approved by the Institutional Animal Care and Use Committee of East Carolina University (Assurance A3469-01).

2.2 | Imaging

Single-molecule RNA in situ hybridization (smFISH) was performed on whole brains of adult mice using the HiPlex RNAscope, as previously described (Fernandez et al., 2021). Detection of smFISH was performed using the RNAscope HiPlex Alternative Display Module (cat. no. 30040), and the DAPI counterstain by an AxioImager MI microscope with objectives of 20x/0.8 NA and 63x/1.3 NA and an AxioCam MRm (Carl Zeiss Microscopy). All images were combined using the RNAscope HiPlex registration Software (cat. no. 300065). As a positive control, a panel of housekeeping gene mRNAs was probed (RNAscope HiPlex12 Positive Control Probe, catalog 324 321), and an irrelevant bacterial gene served as a negative control (ACD cat. no. 324341).

2.3 | Immunofluorescence

Three-month-old mouse brain samples were fixed in 4% paraform-aldehyde for 24 h and placed in 30% sucrose for 24 h. Samples were then embedded in OCT mounting media overnight (Sakura Finetek USA, Torrance, CA, USA), flash frozen, and cryosectioned into 10-μm-thick sections. Antigen retrieval was performed before staining, using citrate-based Antigen Unmasking Solution (Vector Laboratories, cat. no. H-3300). Cryosections were incubated in PBS for 5 min, then 5% normal goat serum in PBS blocking solution for 1 h at room temperature. After normal goat serum blocking was completed, cryosections were incubated with 5% M.O.M. blocking reagent (Vector Laboratories, cat. no. MKB-2213-1) in PBS for 1 h at room temperature. Primary antibodies were diluted in 2% normal goat serum in PBS, added to fixed cultures, and kept at 4°C overnight (Tyrosine Hydroxylase: 1:10 000, Millipore-Sigma, cat. no. ab152; Anti-Flag M2 1:750, Sigma Aldrich cat. no. F3165). After three PBS washes, secondary antibodies diluted in 2% normal goat serum in PBS were added to fixed cultures and kept at room temperature for 1 h (Alexa Fluor 488-conjugated Donkey Anti-Rabbit IgG, 1:500, Jackson Immuno Research cat. no. 711–545-152; Goat anti-Mouse IgG, Alexa Fluor 647, 1:500, Invitrogen cat. no. A-21235). Cryosections were mounted using DAPI mounting medium. TH and ACSL6 immunofluorescent images were acquired on a ZEISS LSM 800 confocal microscope at 63× total magnification, using the 639, 488, and 405 channels. Z-stacked images were acquired, five images across 5 μm, and used to generate maximum intensity orthogonal projections. The pixel resolution is 0.050 μm per pixel (10). *Lipidomics and metabolomics*: MALDI lipid imaging was performed on 10 μm slices of flash-frozen unfixed tissue by the Translational Analytical core of the National Institute on Drug Abuse Intramural Research Program using a Thermo Scientific MALDI LTQ-XL-Orbitrap (Thermo Fisher Scientific), as described (Fernandez et al., 2021; Hale et al., 2019). Xcalibur software (Thermo Fisher Scientific) was used in positive and negative ion mode with a mass resolution of 60 000 in the mass range of 600–1000 Da and a raster step size of 40 μm in both the X and Y directions. Assignment of the lipid species identity was determined using accurate mass with an error of two or less parts per million (ppm) and 3.5 or less ppm in the positive and negative ion modes, respectively. Lipidomics was performed by Purdue University's Bindley Bioscience Center Metabolite Profiling facility using Broad MRM-based lipid profiling, as previously described (Fernandez et al., 2018, 2021). Briefly, lipid extraction from tissues was performed using the Bligh and Dyer method (Bligh & Dyer, 1959). Using a micro-autosampler (G1377A), dried and resuspended lipid phase was injected into a QQQ6410 triple-quadrupole mass spectrometer in positive ion mode and equipped with a Jet Stream electrospray ionization ion source (Agilent Technologies). Analysis was done using the LipidMaps database by calculating the percent distribution for each ion. *Metabolites*: polar phase of the extraction method described above was dried, resuspended, and injected directly into a QQQ6410 triple quadrupole mass spectrometer (Agilent Technologies, San Jose, CA) using the instrument conditions described previously (Pereyra et al., 2020). This is a first-pass exploratory method with direct injection. Therefore, the attributions are tentative and the molecular structure of the MRMs presenting higher intensity compared to the blank sample was not confirmed.

2.4 | Neurochemistry

Neurochemistry of control and Acsl6$^{DA-/-}$ dopamine and serotonin metabolite striatum samples sent to the Vanderbilt University Neurochemistry Core, as described (Wong et al., 2016; Yohn et al., 2020). Tissues were homogenized, using a tissue dismembrator, in 100–750 μL of 0.1 M TCA, which contained 10–2 M sodium acetate, 10–4 M EDTA, and 10.5% methanol (pH 3.8). Ten microliters of homogenate was used for protein quantification using BCA Protein Assay Kit (Thermo Scientific, Waltham, MA USA). Samples were spun in a microcentrifuge at 10 000 g for 20 min at 4°C. The supernatant was removed for LC/MS analysis. Analytes in tissue extract supernatant were quantified using liquid chromatography/mass spectrometry (LC/MS) following derivatization with benzoyl chloride (BZC). Five microliters of supernatant was then mixed with 10 μm each of 500 mM NaCO3 (aq) and 2% BZC in acetonitrile in an LC/MS vial. After 2 min, the reaction was stopped by the addition of a 10μL internal standard solution. LC was performed on a 2.1 × 100 mm, 1.6 μm particle CORTECS Phenyl column (Waters Corporation, Milford, MA, USA) using a Waters Acquity UPLC. Mobile phase A was 0.1% aqueous formic acid and mobile phase B was acetonitrile with 0.1% formic acid. MS analysis was performed using a Waters Xevo TQ-XS triple quadrupole tandem mass spectrometer. The source temperature was 150°C, and the desolvation temperature was 400°C.

For control and Acsl6$^{-/-}$ dataset, the striatum samples were processed similar to (Agim & Cannon, 2018; O'Neal et al., 2014; Wang et al., 2014) for neurotransmitter analyses through high-performance liquid chromatography (HPLC) system with a Dionex Ultimate 3000 Model ISO-31000BM pump, a model WPS-3000TBSL autosampler, Coulochem III electrochemical detector, and an ESA Coulochem data station (ThermoScientific, Waltham, MA). Brain samples were separated on a Waters XBridge reverse phase C18 column (150 × 3.0 mm, 3.5 μm particle size) (Waters Corp, Milford, MA). For monoamine separation, the mobile phase was: 80 mM NaH2PO4, 10% methanol, 2 mM octanesulfonic acid, 0.025 mM ethylenediaminetetraacetic acid, and 0.2 mM trimethylamine, at pH 2.4. Monoamines were detected by analytical cell set at E1 = −150 mV and E2 = +350 mV. The levels of neurotransmitters tested here were calculated using the area under the curve by comparison with a standard curve. Levels were normalized to total protein amount (ng neurotransmitter/mg protein) using BCA Protein Assay Kit (Thermo Scientific, Waltham, MA, USA).

2.5 | Molecular

Total RNA was isolated from striatum using TRIzol (Life Technologies) and quantified using the NanoDrop 1000 spectrophotometer (Thermo Fisher Scientific). High-Capacity cDNA Reverse Transcriptase (Applied Biosystems) was used to generate cDNA. Real-time PCR (RT-PCR) was performed with Sybr Green Master Mix (BioRad) on the QuantStudio 3 Real-Time PCR System (Applied Biosystems).

2.6 | Behavior

For circadian cycle experiments, mice were individually housed in cages containing a monitored, rotating wheel, with access to food and water. Six cages were contained in a light-impenetrable cabinet. Light cycles were manually adjusted in 2-week intervals starting

with a 12-h light/dark cycle, with darkness from 1930 to 0730 to acclimate the mice to the new environment and obtain baseline activity data. The cycle was then shifted 6 h earlier with a dark cycle from 1330 to 0130 to emulate jet lag. Mice were then maintained in 24-h darkness to determine the free-running period (Partington et al., 2021). All activities within the cabinets were monitored and quantified using ClockLab software (Actimetrics, Wilmette, IL). The activity onset was defined with the ClockLab software as the first bin above a threshold of five counts preceded by at least 6 h of inactivity and followed by at least 6 h of activity, in some cases of sporadic activity behavior, the onset was determined manually using similar parameters. For photoentrainment, the ClockLab software combined with blinded manual analyses were used to calculate the time of onset of wheel running determined on the day in which activity onset was within 15 min of the time the lights went off. To assess spatial working memory, mice were subjected to a Y-maze spontaneous alteration test. Mice were brought into the testing room at about 8 am 30 min before the test to acclimate to the new environment. Y-maze was conducted by placing a mouse in a Y-shaped maze with three arms of equal length and allowing the mouse to move freely for 5 min. The percentage of spontaneous alteration was calculated by dividing the number of total alterations by the total number of triads [spontaneous alteration = (total alterations/(total entries-2))×100] as described (Fernandez et al., 2021). Investigators were blinded to genotype during testing and data analysis.

2.7 | Statistical analysis

Power was calculated using G*power software by F tests for one-way ANOVA with an effect size of 0.3 for 90% power. Data are shown as the mean ± SEM for each group unless otherwise stated. Each data point indicates a biological replicate. Data were analyzed using Prism 9.0 software (GraphPad). The statistical significance was determined using a two-tailed Student's *t*-test and set at $p < 0.05$. Outliers were identified using Grubb's test. Data were not assessed for normality. For the Y-maze, two mice were identified as outliers and three mice were excluded from the analysis because they spent >2 min in the same arm. For the circadian cycle experiments, four mice were excluded from the analysis because they did not run on the wheel.

3 | RESULTS

3.1 | ACSL6 is expressed in dopaminergic neurons

Ambulatory activity is known to be controlled, in part, by dopamine. Therefore, we questioned if the hyperactivity of *Acsl6*$^{-/-}$ mice (Fernandez et al., 2018, 2021) could be regulated by ACSL6 action within dopaminergic neurons. First, we confirmed *Acsl6* mRNA expression within dopaminergic neurons of the substantia nigra using smFISH (Figure 1a). Tyrosine hydroxylase (Th) was used as a marker of active dopaminergic neurons. A high degree of co-localization between *Acsl6* (green) and *Th* (red) transcript was indicated by yellow puncta (Figure 1a). As a negative control, no yellow rounded puncta were observed in the *Acsl6*$^{-/-}$ mice (Figure 1a). Non-specific yellow oblong-shaped signal outside our region of interest was a commonly observed auto-fluorescent artifact found in all channels in brain smFISH. Acsl6 expression in dopaminergic neurons was further confirmed by targeting protein expression by immunofluorescence. Specifically, mice expressing a Flag-

tag ligated to endogenous ACSL6 showed that ACSL6-flag colocalized with TH (Figure 1b). These data demonstrate ACSL6 expression in midbrain dopaminergic neurons.

3.2 | ACSL6 is required for membrane unsaturation in striatal dopaminergic innervations

The role of ACSL6 in regulating membrane lipid composition in brain regions innervated by dopaminergic neurons was assessed by lipidomic profiling on the striatum because of its high density of dopaminergic neuronal terminals and projections. Lipidomic profiling on several brain regions, including the cortex, midbrain, hippocampus, and cerebellum, has demonstrated similar lipid alterations because of ACSL6 deficiency (Fernandez et al., 2018), herein the striatum was compared to the cerebellum. Similar to the cerebellum, the *Acsl6*$^{-/-}$ striatum was depleted of DHA-enriched phosphatidylcholine (PC) species, specifically PC 38:6, 40:6, and 40:7 were reduced ~50% (Figure 2a). Similar to the cerebellum, several PCs containing two double bonds were increased in *Acsl6*$^{-/-}$ striatum (Figure 2a). However, while *Acsl6*$^{-/-}$ cerebellum had increased levels of PCs with 3, 4, and 5-double bonds compared to controls, these species in the striatum were either unchanged or decreased by ACSL6 loss (Figure 2a). These data demonstrated that when membrane DHA is depleted by ACSL6 loss, the cerebellum compensates by increasing the content of other polyunsaturated fatty acids (PUFAs), whereas the striatum did not show increases in other PUFAs for PCs. To highlight this distinction, the relative change between control and *Acsl6*$^{-/-}$ for several phospholipid species was compared between the cerebellum and striatum demonstrating a dichotomy in membrane unsaturation between the two brain regions, particularly for 3- and 4-double bond containing PCs, in *Acsl6*$^{-/-}$ mice (Figure 2b). The reduction of DHA-enriched phospholipids was reflected across phosphatidylethanolamine, phosphatidylserine, and phosphatidylinositol (Figure 2c). Interestingly, decreased 4-double bond phospholipids were only observed for PC, whereas phosphatidylethanolamine and phosphatidylserine had increased, and phosphatidylinositol showed no change (Figure 2c). To provide a visual representation of the distinct nature and spatial distribution of genotype-driven alterations in cerebellar compared to striatal lipids, MALDI-based lipid imaging was performed. In agreement with the lipidomic data, MALDI lipid imaging of the DHA-enriched PC38:6 and PC40:6 species was depleted in *Acsl6*$^{-/-}$ cerebellum compared to controls (Figure 2d,e). However, arachidonic acid (AA)-enriched PC38:4 and PC36:4 species showed higher signal in *Acsl6*$^{-/-}$ cerebellum compared to controls. Conversely, in the striatum of *Acsl6*$^{-/-}$ compared to controls, both the DHA-enriched and the AA-enriched PCs were depleted (Figure 2d,e). These data confirm that ACSL6 is critical for regulating membrane PUFA content in the dopaminergic-innervation-rich striatum. These data also suggest that the *Acsl6*$^{-/-}$ striatum, unlike the cerebellum, was overall depleted of membrane PUFAs.

We previously found that *Acsl6*$^{-/-}$ cerebellum had decreased gene expression of several synaptic proteins and that *Acsl6*$^{-/-}$ had altered expression of genes regulating glutamate metabolism, as well as lower glutamate abundance (Fernandez et al., 2018, 2021). However, no differences were detected in the synaptic or glutamate-related genes in the *Acsl6*$^{-/-}$ striatum (Figure 3a). Assessment of dopamine-related genes in the *Acsl6*$^{-/-}$ striatum, compared to controls, showed a significant decrease in dopamine receptor D1 (Drd1), the most abundant dopamine receptor in the central nervous system (Figure 3b). Neurochemically, dopamine and its metabolites trended to be decreased while dopamine

turnover was increased in *Acsl6*$^{-/-}$ striatum (Figure 3c,d). Together, these data suggest that loss of ACSL6 alters the lipidome and metabolism of dopaminergic neurons.

3.3 | Loss of ACSL6 specifically in dopaminergic neurons regulates striatal neurochemistry

ACSL6 is expressed in both neurons and astrocytes throughout the CNS, with a particular ability to enrich neurons, but not astrocytes, with PUFAs (Fernandez et al., 2021). To determine if ACSL6 specifically found within dopaminergic neurons was critical for regulating dopaminergic homeostasis, *Acsl6* floxed conditional knockout mice were bred with mice expressing Cre recombinase driven by the dopamine transporter promoter to generate a mouse model of ACSL6 depletion exclusively in dopaminergic neurons (*Acsl6*$^{DA-/-}$). ACSL6 loss in dopaminergic neurons resulted in reduced levels of the dopamine intermediary metabolite, DOPAC, and reduced dopamine turnover in the striatum (Figure 4a–c). Omega-3 fatty acid levels correlate with both dopamine and serotonin (Hibbeln et al., 1998) and as such serotonin levels were significantly reduced in the *Acsl6*$^{DA-/-}$ striatum (Figure 4d). The gene expression of dopaminergic receptors was unchanged except for an increase in Drd3 and a trending increase in Th (Figure 4e). The complete knockout of ACSL6 resulted in increased expression of genes regulated by the sterol regulatory element binding protein (SREBP) (Fernandez et al., 2021). In congruence, the *Acsl6*$^{DA-/-}$ striatum showed increased expression of SREBP target genes (Figure 4f). Metabolite analysis of control compared to *Acsl6*$^{DA-/-}$ striatum revealed several increased levels of amino acids and the highly abundant neurotransmitter glutamate (Figure 4g,h). Together, these data suggest that loss of ACSL6 specifically in dopaminergic neurons perturbs striatal dopaminergic homeostasis, metabolism, and neurotransmitter abundance.

3.4 | Dopaminergic ACSL6 is required for recovery from photoperiod entrainment

The complete loss of dopamine transporter in mice impairs response in the Y-maze challenge suggesting the requirement of dopamine during this test (Li et al., 2010). The Y-maze tests several regions of the brain, including the hippocampus, septum, basal forebrain, and prefrontal cortex. The germline deletion of ACSL6 resulted in increased arm entries and a reduced percentage of spontaneous alternations as previously reported (Fernandez et al., 2021), suggesting hyperlocomotion and poor spatial learning and memory in ACSL6 deficiency (Figure 5a–c). However, the exclusive loss of ACSL6 in dopamine transporter-expressing cells did not have a significant impact on arm entries or the percentage of spontaneous alternations during Y-maze (Figure 5d–f). These data suggest that ACSL6's role in regulating responses to the Y-maze is not dependent on ACSL6 expression exclusively within dopaminergic neurons.

Dopaminergic control was next assessed in relation to light-cycle regulation of physical activity as a measure of the role of dopamine in circadian control (Grippo & Guler, 2019; Mendoza & Challet, 2014; Partington et al., 2021). The activity was monitored in light-controlled housing chambers containing running wheels. Daily patterns of wakefulness onset and duration were indicated by monitoring wheel-running activity. Mice were acclimated to the housing environment until the daily onset of activity was stable. While the time of daily onset of activity during the dark cycle was not genotypically different, the *Acsl6*$^{DA-/-}$

mice exhibited hyperlocomotion by increased wheel activity compared to controls during the dark cycle (Figure 6a). These data agree with the hyperlocomotion observed in *Acsl6*$^{-/-}$ (Fernandez et al., 2021) and suggest that hyperlocomotion outcomes in home cages with access to a running wheel are driven, in part, by the loss of ACSL6 in dopaminergic neurons. After mice had adjusted to the home-cage environment, entrainment to a 6-h earlier shift in the dark cycle was assessed to mimic a jetlag-like scenario. Hyperlocomotion continued to be observed in *Acsl6*$^{DA-/-}$ mice after jetlag initiation (Figure 6c). The number of days required for the animals to consistently initiate wheel running, at least 5 h prior to the jetlag initiation, was used to determine days to entrainment. Littermate control mice adjusted to the light entrainment in ~6 days, yet both *Acsl6*$^{-/-}$ and *Acsl6*$^{DA-/-}$ mice required additional days to adjust to the shift in light cycle (Figure 6d). Specifically, *Acsl6*$^{-/-}$ mice required ~10 days, and *Acsl6*$^{DA-/-}$ required ~8 days to recover from a 6-h shift in the light cycle (Figure 6e,f). Hyperlocomotion and poor recovery from light entrainment were observed in male, but not female *Acsl6*$^{DA-/-}$ mice suggesting a sexual dichotomy for ACSL6-directed regulation of dopaminergic control during circadian rhythms (Figure S1). No differences in the average free-running period were detected in either *Acsl6*$^{-/-}$ or *Acsl6*$^{DA-/-}$ mice. Together, the poor recovery to a jetlag-like shift in the light cycle of male dopaminergic ACSL6-deficient mice suggests that ACSL6 is required for proper circadian adaptations because of perturbations in the light cycle.

4 | DISCUSSION

Dopamine transmission fluctuates with circadian rhythmicity and is influenced by the light/dark cycle (Partington et al., 2021). In nocturnal mice, over a 12-h light/dark cycle, dopamine transmission peaks midway through the active/dark cycle and is at its lowest midway through the sleep/light cycle. Regulators of dopamine circadian fluctuations include Nurr1, a nuclear transcription factor important for the dopaminergic activity of a neuron and for the sensitivity to altered photoentrainment (Partington et al., 2021). Indeed, the hemizygous deletion of Nurr1 in mice results in reduced expression of dopamine-related genes such as tyrosine hydroxylase and dopamine transporter along with increased activity in the open field, increased sensitivity to amphetamine, and decreased wheel running (Eells et al., 2015; Moore et al., 2008; Partington et al., 2021). Here, ACSL6 deficiency in dopaminergic neurons induced hyperactivity, and while it did not influence circadian rhythms under basal conditions, it decreased circadian recovery in response to a jetlag mimetic. The mechanisms driving these effects are less likely related to a role for ACSL6 in transcriptional control of dopaminergic circadian fluctuations, but more likely related to membrane-influenced outcomes. Specifically, altering DHA content in membranes is known to reduce membrane budding rates, decrease membrane packing defects, and repress the activity of membrane-bound proteins (Manni et al., 2018). Within neuronal membranes, the synapse is the most DHA-dense region (Barelli & Antonny, 2016; Cao et al., 2009). Loss of ACSL6 and low levels of DHA in membranes results in reduced expression of synaptic-related genes (Fernandez et al., 2021). Specifically, within the context of dopaminergic neurons, variations in omega-3 fatty acid levels are positively correlated with dopamine metabolite concentrations and the abundance of dopamine receptors (Bondi et al., 2014; Metz et al., 2019; Zimmer et al., 2002). The loss of ACSL6 at either the total body level

or only in dopamine neurons reduced dopamine receptor mRNA abundance for Drd1 and increased Drd3 in the striatum, respectively (Figure 4), suggesting an impact of ACSL6 on dopamine receptor transcriptional control in this brain region. In humans, omega-3 content in the cerebrospinal fluid is positively correlated with both dopamine and serotonin metabolites (Hibbeln et al., 1998; Sublette et al., 2014). However, depressive disorder patients show inverse correlations between plasma omega-3 s and dopamine metabolites, but not for serotonin (Sublette et al., 2014). Alzheimer's disease models also show an inverse relationship between omega-3 deficiency and poor health and metabolic outcomes related to the dopaminergic system (Belkouch et al., 2016; Cardoso et al., 2016; Patrick, 2019). As such, the loss of ACSL6 in dopamine neurons reduced striatal dopamine metabolite levels, dopamine turnover rates, and serotonin levels (Figure 4). These data suggest that the role of ACSL6 in omega-3 fatty acid metabolism in dopamine neurons impacts serotonin and dopaminergic homeostasis in a manner consistent with the correlations between omega-3 status to these neurotransmitters. Broadly, the impact of omega-3 s on dopamine is linked to outcomes of schizophrenia, ADHD, depression, and Parkinson's disease (Chang et al., 2018; Das, 2013; Dervola et al., 2012; Frajerman et al., 2021; Grosso et al., 2014; Sublette et al., 2014). ACSL6 and neuronal DHA metabolism is shown to be altered in schizophrenia, ADHD, depression, and Parkinson's disease suggesting that the metabolic control regulated by ACSL6 may play a key role in linking omega-3 fatty acid metabolism to these diseases and disorders (Chen et al., 2011; Kurotaki et al., 2011; Luo et al., 2008).

The sex-specific responses to the loss of ACSL6 in dopaminergic neurons suggest a sex-dependent relationship between lipid metabolism and dopaminergic control. There is a precedence for sex-specific responses of DHA-linked dopaminergic control. Specifically, spontaneously hypertensive rats fed with or without dietary DHA demonstrated significant changes in dopamine metabolism by dietary DHA in males but not in females (Dervola et al., 2012). Clinical, animal, and epidemiological data suggest sex-specific differences in DHA content, response to dietary manipulations, and health outcomes but the mechanisms and nuances remain to be well established (Ghasemi Fard et al., 2019). Herein, we demonstrate that ACSL6 in dopaminergic neurons alters dopamine metabolism and regulation of the circadian cycle suggesting that the DHA metabolism mediated by ACSL6 plays a role in dopamine neuron biology.

Dopaminergic neuronal function is important in Parkinson's disease (PD), a disease well characterized to involve the loss and/or dysfunction of dopaminergic neurons. The intake of omega-3 polyunsaturated fatty acids such as DHA is inversely correlated with the risk of PD in the general population and in populations exposed to pesticides known to promote PD risk (de Lau et al., 2005; Kamel et al., 2014). In agreement, animal models have demonstrated that lower dietary omega-3 s intake is associated with negative outcomes driven by dopaminergic neurons (Zimmer et al., 1998). For instance, dietary omega-3 PUFAs improve outcomes in the 6-hydroxydopamine lesion (Chitre et al., 2020), MPTP-induced (Hacioglu et al., 2012; Ozsoy et al., 2011; Parlak et al., 2018), and rotenone-induced models of PD (Oguro et al., 2021). Alpha-synuclein accumulates and aggregates in an abnormal manner in patients affected with PD (De Franceschi et al., 2009, 2011; Dhakal et al., 2021; Fecchio et al., 2018). As such, much research and modeling of PD has focused on alpha-synuclein biology. Surprisingly, in a mouse model of synucleinopathy where human

alpha-synuclein containing the PD-linked A53T mutation is over-expressed, dietary DHA increases negative outcomes (Yakunin et al., 2012). Thus, the question remains as to the beneficial or deleterious nature of DHA in PD pathobiology.

Supplementary Material

Refer to Web version on PubMed Central for supplementary material.

ACKNOWLEDGMENTS

This work was supported by the Lina Mae Edwards Young Investigator Award from the Dementia Alliance of North Carolina and NIH grants R01 HD090007 and U01 DA054170 to BPH. This research was supported, in part, by the Translational Analytical Core of the Intramural Research Program of the National Institute on Drug Abuse, NIH. Experimental timeline image generated in Biorender.com.

DATA AVAILABILITY STATEMENT

Data sharing not applicable to this article as no datasets were generated or analyzed during the current study

Abbreviations:

AA	arachidonic acid
ACSL6	long-chain acyl-CoA synthetase 6
DA	dopamine
DHA	docosahexaenoic acid
PC	phosphatidylcholine
PD	Parkinson’s disease
PUFA	polyunsaturated fatty acid
smFISH	Single-molecule RNA in situ hybridization
TH	Tyrosine hydroxylase

REFERENCES

Agim ZS, & Cannon JR (2018). Alterations in the nigrostriatal dopamine system after acute systemic PhIP exposure. Toxicology Letters, 287, 31–41. [PubMed: 29378243]

Barelli H, & Antonny B (2016). Lipid unsaturation and organelle dynamics. Current Opinion in Cell Biology, 41, 25–32. [PubMed: 27062546]

Belkouch M, Hachem M, Elgot A, Lo Van A, Picq M, Guichardant M, Lagarde M, & Bernoud-Hubac N (2016). The pleiotropic effects of omega-3 docosahexaenoic acid on the hallmarks of Alzheimer’s disease. The Journal of Nutritional Biochemistry, 38, 1–11. [PubMed: 27825512]

Beninger RJ (1983). The role of dopamine in locomotor activity and learning. Brain Research, 287(2), 173–196. [PubMed: 6357357]

Bligh EG, & Dyer WJ (1959). A rapid method of total lipid extraction and purification. Canadian Journal of Biochemistry and Physiology, 37, 911–917. [PubMed: 13671378]

Bondi CO, Taha AY, Tock JL, Totah NK, Cheon Y, Torres GE, Rapoport SI, & Moghaddam B (2014). Adolescent behavior and dopamine availability are uniquely sensitive to dietary omega-3 fatty acid deficiency. Biological Psychiatry, 75(1), 38–46. [PubMed: 23890734]

Cao D, Kevala K, Kim J, Moon HS, Jun SB, Lovinger D, & Kim HY (2009). Docosahexaenoic acid promotes hippocampal neuronal development and synaptic function. Journal of Neurochemistry, 111(2), 510–521. [PubMed: 19682204]

Cardoso C, Afonso C, & Bandarra NM (2016). Dietary DHA and health: Cognitive function ageing. Nutrition Research Reviews, 29(2), 281–294. [PubMed: 27866493]

Chang JP-C, Su K-P, Mondelli V, & Pariante CM (2018). Omega-3 polyunsaturated fatty acids in youths with attention deficit hyperactivity disorder: A systematic review and meta-analysis of clinical trials and biological studies. Neuropsychopharmacology, 43(3), 534–545. [PubMed: 28741625]

Chen J, Brunzell DH, Jackson K, van der Vaart A, Ma JZ, Payne TJ, Sherva R, Farrer LA, Gejman P, Levinson DF, Holmans P, Aggen SH, Damaj I, Kuo PH, Webb BT, Anton R, Kranzler HR, Gelernter J, Li MD, … Chen X. (2011). ACSL6 is associated with the number of cigarettes smoked and its expression is altered by chronic nicotine exposure. PLoS One, 6(12), e28790. [PubMed: 22205969]

Chitre NM, Wood BJ, Ray A, Moniri NH, & Murnane KS (2020). Docosahexaenoic acid protects motor function and increases dopamine synthesis in a rat model of Parkinson's disease via mechanisms associated with increased protein kinase activity in the striatum. Neuropharmacology, 167, 107976. [PubMed: 32001239]

Crawford MA, Leigh Broadhurst C, Guest M, Nagar A, Wang Y, Ghebremeskel K, & Schmidt WF (2013). A quantum theory for the irreplaceable role of docosahexaenoic acid in neural cell signalling throughout evolution. Prostaglandins, Leukotrienes and Essential Fatty Acids, 88(1), 5–13. [PubMed: 23206328]

Das UN (2013). Polyunsaturated fatty acids and their metabolites in the pathobiology of schizophrenia. Progress in Neuro-Psychopharmacology and Biological Psychiatry, 42, 122–134. [PubMed: 22735394]

De Franceschi G, Frare E, Bubacco L, Mammi S, Fontana A, & de Laureto PP (2009). Molecular insights into the interaction between α-Synuclein and docosahexaenoic acid. Journal of Molecular Biology, 394(1), 94–107. [PubMed: 19747490]

De Franceschi G, Frare E, Pivato M, Relini A, Penco A, Greggio E, Bubacco L, Fontana A, & de Laureto PP (2011). Structural and morphological characterization of aggregated species of α-Synuclein induced by docosahexaenoic acid. Journal of Biological Chemistry, 286(25), 22262–22274. [PubMed: 21527634]

de Lau LM, Bornebroek M, Witteman JC, Hofman A, Koudstaal PJ, & Breteler MM (2005). Dietary fatty acids and the risk of Parkinson disease: The Rotterdam study. Neurology, 64(12), 2040–2045. [PubMed: 15985568]

Dervola KS, Roberg BA, Wøien G, Bogen IL, Sandvik TH, Sagvolden T, Drevon CA, Johansen EB, & Walaas SI (2012). Marine O-3 polyunsaturated fatty acids induce sex-specific changes in reinforcer-controlled behaviour and neurotransmitter metabolism in a spontaneously hypertensive rat model of ADHD. Behavioral and Brain Functions, 8, 56. [PubMed: 23228189]

Dhakal S, Saha J, Wyant CE, & Rangachari V (2021). αS oligomers generated from interactions with a polyunsaturated fatty acid and a dopamine metabolite differentially interact with Aβ to enhance neurotoxicity. ACS Chemical Neuroscience, 12(21), 4153–4161. [PubMed: 34665617]

Eells JB, Varela-Stokes A, Guo-Ross SX, Kummari E, Smith HM, Cox AD, & Lindsay DS (2015). Chronic toxoplasma gondii in Nurr1-null heterozygous mice exacerbates elevated open field activity. PLoS One, 10(4), e0119280. [PubMed: 25855987]

Ellis JM, Frahm JL, Li LO, & Coleman RA (2010). Acyl-coenzyme a synthetases in metabolic control. Current Opinion in Lipidology, 21(3), 212–217. [PubMed: 20480548]

Fecchio C, Palazzi L, & de Laureto PP (2018). α-Synuclein and polyunsaturated fatty acids: Molecular basis of the interaction and implication in neurodegeneration. Molecules, 23(7), 1531. [PubMed: 29941855]

Fernandez RF, & Ellis JM (2020). Acyl-CoA synthetases as regulators of brain phospholipid acyl-chain diversity. Prostaglandins, Leukotrienes and Essential Fatty Acids, 161, 102175. [PubMed: 33031993]

Fernandez RF, Kim SQ, Zhao Y, Foguth RM, Weera MM, Counihan JL, Nomura DK, Chester JA, Cannon JR, & Ellis JM (2018). Acyl-CoA synthetase 6 enriches the neuroprotective omega-3 fatty acid DHA in the brain. Proceedings of the National Academy of Sciences of the United States of America, 115(49), 12525–12530. [PubMed: 30401738]

Fernandez RF, Pereyra AS, Diaz V, Wilson ES, Litwa KA, Martínez-Gardeazabal J, Jackson SN, Brenna JT, Hermann BP, Eells JB, & Ellis JM (2021). Acyl-CoA synthetase 6 is required for brain docosahexaenoic acid retention and neuroprotection during aging. JCI Insight, 6(11), 144351.

Frajerman A, Scoriels L, Kebir O, & Chaumette B (2021). Shared biological pathways between antipsychotics and Omega-3 fatty acids: A key feature for schizophrenia preventive treatment? International Journal of Molecular Sciences, 22(13), 6881. [PubMed: 34206945]

Ghasemi Fard S, Wang F, Sinclair AJ, Elliott G, & Turchini GM (2019). How does high DHA fish oil affect health? A systematic review of evidence. Critical Reviews in Food Science and Nutrition, 59(11), 1684–1727. [PubMed: 29494205]

Grevengoed TJ, Martin SA, Katunga L, Cooper DE, Anderson EJ, Murphy RC, & Coleman RA (2015). Acyl-CoA synthetase 1 deficiency alters cardiolipin species and impairs mitochondrial function. Journal of Lipid Research, 56(8), 1572–1582. [PubMed: 26136511]

Grippo RM, & Güler AD (2019). Dopamine signaling in circadian photoentrainment: Consequences of desynchrony. The Yale Journal of Biology and Medicine, 92(2), 271–281. [PubMed: 31249488]

Grosso G, Pajak A, Marventano S, Castellano S, Galvano F, Bucolo C , Drago F, & Caraci F (2014). Role of Omega-3 fatty acids in the treatment of depressive disorders: A comprehensive meta-analysis of randomized clinical trials. PLoS One, 9(5), e96905. [PubMed: 24805797]

Guixà-González R, Javanainen M, Gómez-Soler M, Cordobilla B, Domingo JC, Sanz F, Pastor M, Ciruela F, Martinez-Seara H, & Selent J (2016). Membrane omega-3 fatty acids modulate the oligomerisation kinetics of adenosine A2A and dopamine D2 receptors. Scientific Reports, 6(1), 19839. [PubMed: 26796668]

Hacioglu G, Seval-Celik Y, Tanriover G, Ozsoy O, Saka-Topcuoglu E, Balkan S, & Agar A (2012). Docosahexaenoic acid provides protective mechanism in bilaterally MPTP-lesioned rat model of Parkinson's disease. Folia Histochemica et Cytobiologica, 50(2), 228–238. [PubMed: 22763967]

Hale BJ, Fernandez RF, Kim SQ, Diaz VD, Jackson SN, Liu L, Brenna JT, Hermann BP, Geyer CB, & Ellis JM (2019). Acyl-CoA Synthetase 6 enriches seminiferous tubules with the omega-3 fatty acid DHA and is required for male fertility in the mouse. Journal of Biological Chemistry, 294, 14394–14405. [PubMed: 31399511]

Hibbeln JR, Linnoila M, Umhau JC, Rawlings R, George DT, & Salem N Jr. (1998). Essential fatty acids predict metabolites of serotonin and dopamine in cerebrospinal fluid among healthy control subjects, and early- and late-onset alcoholics. Biological Psychiatry, 44(4), 235–242. [PubMed: 9715354]

Kamel F, Goldman SM, Umbach DM, Chen H, Richardson G, Barber MR, Meng C, Marras C, Korell M, Kasten M, Hoppin JA, Comyns K, Chade A, Blair A, Bhudhikanok GS, Webster Ross G, William Langston J, Sandler DP, & Tanner CM (2014). Dietary fat intake, pesticide use, and Parkinson's disease. Parkinsonism & Related Disorders, 20(1), 82–87. [PubMed: 24120951]

Kurotaki N, Tasaki S, Mishima H, Ono S, Imamura A, Kikuchi T, Nishida N, Tokunaga K, Yoshiura KI, & Ozawa H (2011). Identification of novel schizophrenia loci by homozygosity mapping using DNA microarray analysis. PLoS One, 6(5), e20589. [PubMed: 21655227]

Li B, Arime Y, Hall FS, Uhl GR, & Sora I (2010). Impaired spatial working memory and decreased frontal cortex BDNF protein level in dopamine transporter knockout mice. European Journal of Pharmacology, 628(1–3), 104–107. [PubMed: 19932884]

Luo X.-j., Diao H.-b., Wang J.-k., Zhang H, Zhao Z.-m., & Su B (2008). Association of haplotypes spanning PDZ-GEF2, LOC728637 and ACSL6 with schizophrenia in Han Chinese. Journal of Medical Genetics, 45(12), 818–826. [PubMed: 18718982]

Manni MM, Tiberti ML, Pagnotta S, Barelli H, Gautier R, & Antonny B (2018). Acyl chain asymmetry and polyunsaturation of brain phospholipids facilitate membrane vesiculation without leakage. eLife, 7, e34394. [PubMed: 29543154]

Marszalek JR, Kitidis C, Dararutana A, & Lodish HF (2004). Acyl-CoA Synthetase 2 overexpression enhances fatty acid internalization and neurite outgrowth. Journal of Biological Chemistry, 279(23), 23882–23891. [PubMed: 15051725]

Mendoza J, & Challet E (2014). Circadian insights into dopamine mechanisms. Neuroscience, 282, 230–242. [PubMed: 25281877]

Metz VG, Segat HJ, Dias VT, Barcelos RCS, Maurer LH, Stiebe J, Emanuelli T, Burger ME, & Pase CS (2019). Omega-3 decreases D1 and D2 receptors expression in the prefrontal cortex and prevents amphetamine-induced conditioned place preference in rats. The Journal of Nutritional Biochemistry, 67, 182–189. [PubMed: 30951972]

Moore TM, Brown T, Cade M, & Eells JB (2008). Alterations in amphetamine-stimulated dopamine overflow due to the Nurr1-null heterozygous genotype and postweaning isolation. Synapse, 62(10), 764–774. [PubMed: 18655117]

Oguro A, Ishihara Y, Siswanto FM, Yamazaki T, Ishida A, Imaishi H, & Imaoka S (2021). Contribution of DHA diols (19,20-DHDP) produced by cytochrome P450s and soluble epoxide hydrolase to the beneficial effects of DHA supplementation in the brains of rotenone-induced rat models of Parkinson's disease. Biochimica et Biophysica Acta–Molecular and Cell Biology of Lipids, 1866(2), 158858. [PubMed: 33279658]

O'Neal SL, Lee JW, Zheng W, & Cannon JR (2014). Subacute manganese exposure in rats is a neurochemical model of early manganese toxicity. Neurotoxicology, 44, 303–313. [PubMed: 25117542]

Ozsoy O, Seval-Celik Y, Hacioglu G, Yargicoglu P, Demir R, Agar A, & Aslan M (2011). The influence and the mechanism of docosahexaenoic acid on a mouse model of Parkinson's disease. Neurochemistry International, 59(5), 664–670. [PubMed: 21736911]

Parlak H, Ozkan A, Dilmac S, Tanriover G, Ozsoy O, & Agar A (2018). Neuronal nitric oxide synthase phosphorylation induced by docosahexaenoic acid protects dopaminergic neurons in an experimental model of Parkinson's disease. Folia Histochemica et Cytobiologica, 56(1), 27–37. [PubMed: 29577226]

Partington HS, Nutter JM, & Eells JB (2021). Nurr1 deficiency shortens free running period, enhances photoentrainment to phase advance, and disrupts circadian cycling of the dopamine neuron phenotype. Behavioural Brain Research, 411, 113347. [PubMed: 33991560]

Patrick RP (2019). Role of phosphatidylcholine-DHA in preventing APOE4-associated Alzheimer's disease. FASEB Journal, 33(2), 1554–1564. [PubMed: 30289748]

Pereyra AS, Rajan A, Ferreira CR, & Ellis JM (2020). Loss of muscle carnitine Palmitoyltransferase 2 prevents diet-induced obesity and insulin resistance despite long-chain Acylcarnitine accumulation. Cell Reports, 33(6), 108374. [PubMed: 33176143]

Sublette ME, Galfalvy HC, Hibbeln JR, Keilp JG, Malone KM, Oquendo MA, & Mann JJ (2014). Polyunsaturated fatty acid associations with dopaminergic indices in major depressive disorder. The International Journal of Neuropsychopharmacology, 17(3), 383–391. [PubMed: 24300434]

Wang Y, Lee J-W, Oh G, Grady SR, McIntosh JM, Brunzell DH, Cannon JR, & Drenan RM (2014). Enhanced synthesis and release of dopamine in transgenic mice with gain-of-function a6* nAChRs. Journal of Neurochemistry, 129(2), 315–327. [PubMed: 24266758]

Wong JM, Malec PA, Mabrouk OS, Ro J, Dus M, & Kennedy RT (2016). Benzoyl chloride derivatization with liquid chromatography-mass spectrometry for targeted metabolomics of neurochemicals in biological samples. Journal of Chromatography A, 1446, 78–90. [PubMed: 27083258]

Yakunin E, Loeb V, Kisos H, Biala Y, Yehuda S, Yaari Y, Selkoe DJ, & Sharon R (2012). α-Synuclein neuropathology is controlled by nuclear hormone receptors and enhanced by docosahexanoic acid in a mouse model for Parkinson's disease. Brain Pathology, 22(3), 280–294. [PubMed: 21929559]

Yohn SE, Foster DJ, Covey DP, Moehle MS, Galbraith J, Garcia-Barrantes PM, Cho HP, Bubser M, Blobaum AL, Joffe ME, Cheer JE, Jones CK, Lindsley CW,& Conn PJ. (2020). Activation of the mGlu(1) metabotropic glutamate receptor has antipsychotic-like effects and is required for

efficacy of M(4) muscarinic receptor allosteric modulators. Molecular Psychiatry, 25(11), 2786–2799. [PubMed: 30116027]

Zimmer L, Hembert S, Durand G, Breton P, Guilloteau D, Besnard JC, SChalon S (1998). Chronic n-3 polyunsaturated fatty acid diet-deficiency acts on dopamine metabolism in the rat frontal cortex: A microdialysis study. Neuroscience Letters, 240(3), 177–181. [PubMed: 9502233]

Zimmer L, Vancassel S, Cantagrel S, Breton P, Delamanche S, Guilloteau D, Durand G, & Chalon S (2002). The dopamine mesocorticolimbic pathway is affected by deficiency in n-3 polyunsaturated fatty acids. The American Journal of Clinical Nutrition, 75(4), 662–667. [PubMed: 11916751]

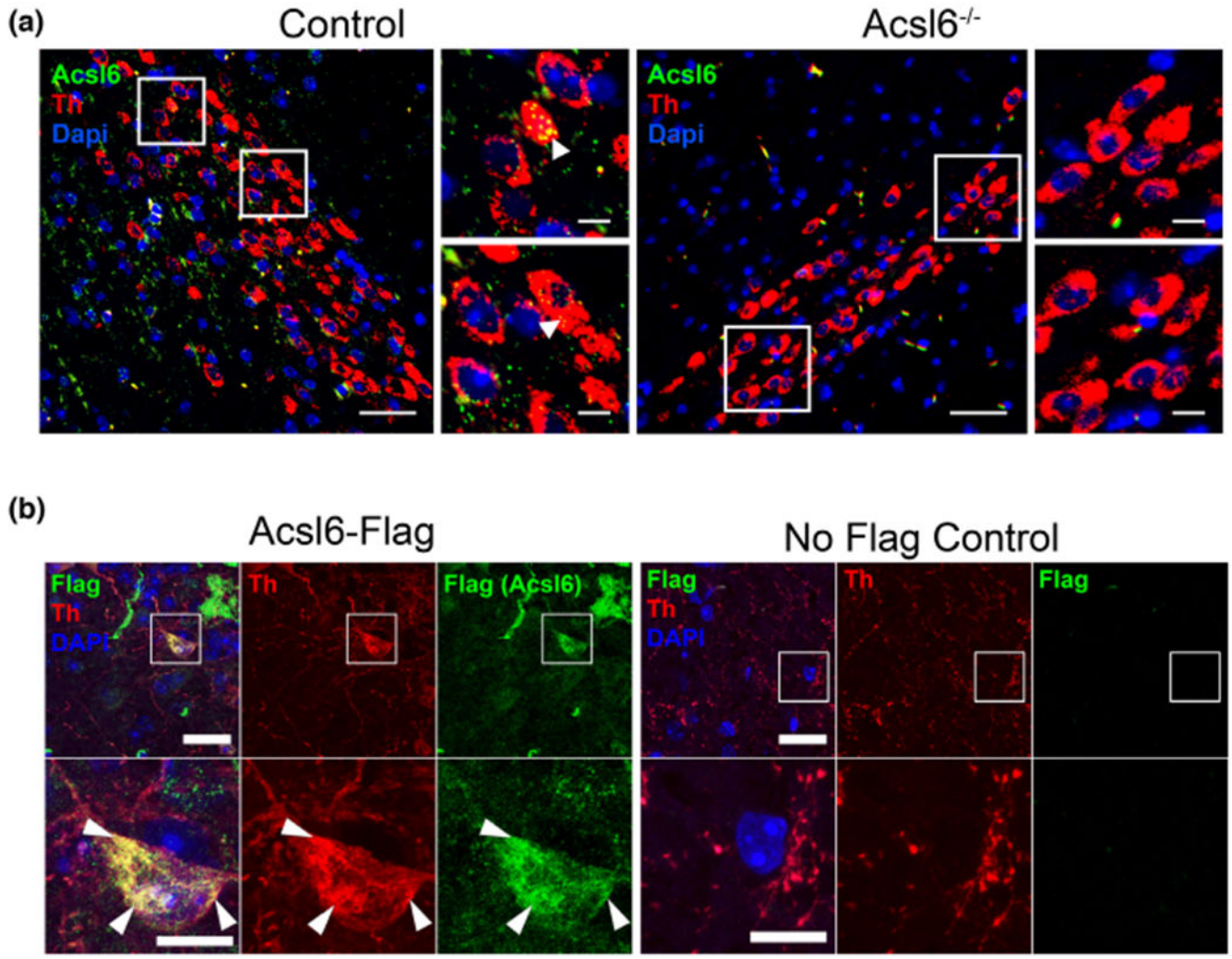

FIGURE 1.

ACSL6 is expressed in dopaminergic neurons. (a) *Acsl6* detection by smFISH in substantial nigra region; Blue: DAPI for nuclei, green: *Acsl6*, red: *Tyrosine hydroxylase, Th, a dopaminergic neuron marker. Acsl6*$^{-/-}$ *serves as a negative control*. Scale bars: 50 or 100 μm. (b) Immunofluorescent confocal images of TH-positive cells (red) and localization of ACSL6-Flag (Anti-FLAG M2 antibody, green), the merged images include nuclei marker DAPI (blue). White-boxed regions of interest highlight individual cells. Left panel: ACSL6-Flag colocalizing in TH-positive cells, bottom panel highlights the region of interest, arrows indicate areas of colocalization. Right panel: TH-positive cells in No-Flag mouse as a negative control. Scale bars: Top: 25 μm, Bottom: 10 μm. Images are representative of two biological replicates.

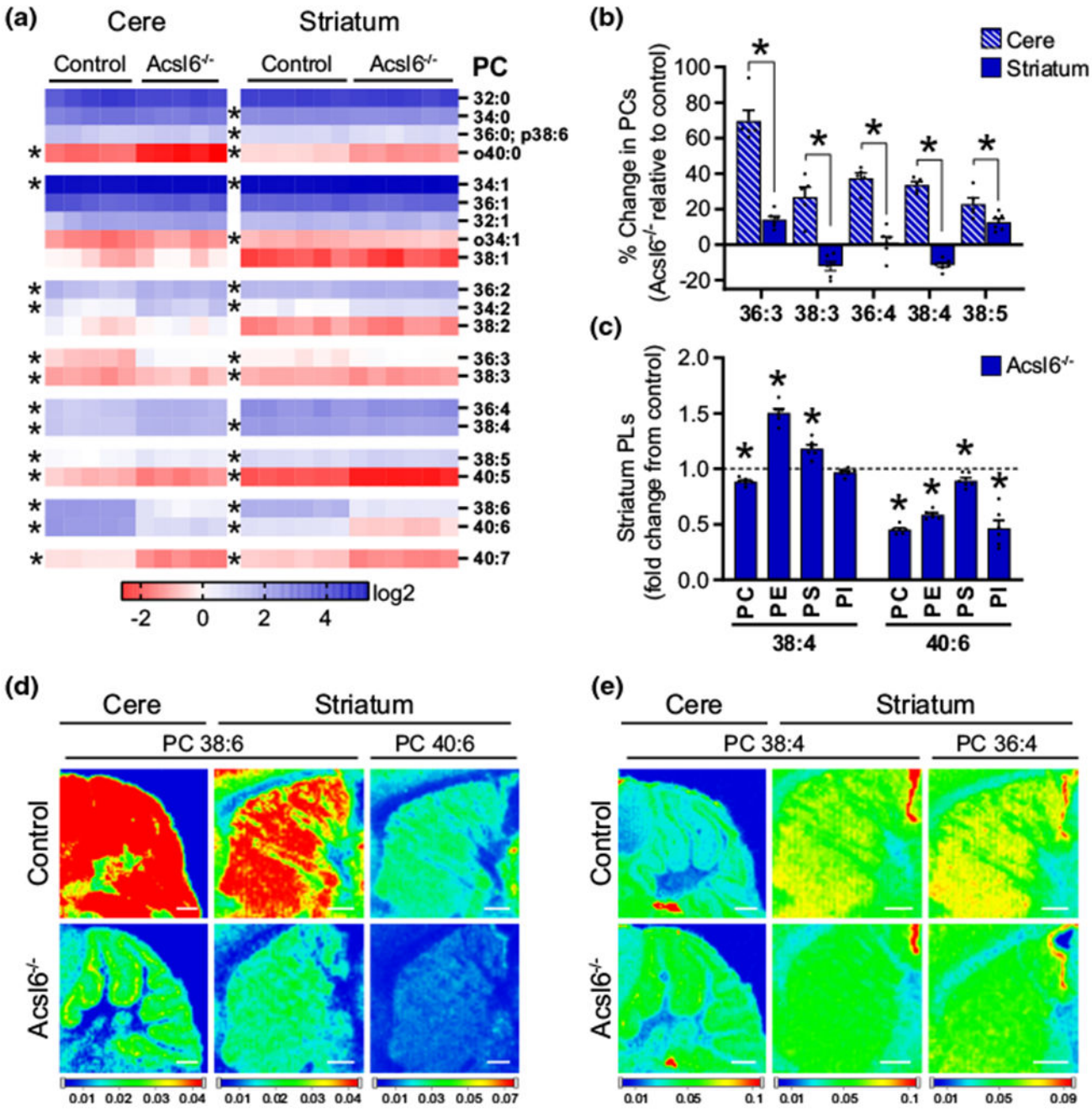

FIGURE 2.

ACSL6 is required for membrane unsaturation in dopaminergic-innervation-rich striatum. (a) Heatmap of PCs clustered by degree of saturation in control and *Acsl6*$^{-/-}$ cerebellum, $n = 5$ or striatum, $n = 6$. Data are presented as % ion intensity distribution, species >0.5% of the total are shown. (b) Percent change between control and *Acsl6*$^{-/-}$ mice for highly abundant PCs with 3 to 5 unsaturated bonds in cerebellum or striatum, $n = 5–6$. (c) Fold-change of total ion count for phosphatidylcholine (PC), phosphatidylethanolamine (PE), phosphatidylserine (PS), and phosphatidylinositol (PI) for phospholipids (PLs) containing

4 or 6 double bonds in the striatum of control or *Acsl6*$^{-/-}$ mice, $n = 6$. Lipid imaging by MALDI of predicted (d) DHA-containing PCs (PC 38:6 m/z = 844.5253 $[M + K]^+$ and PC 40:6 m/z = 872.5566, $[M + K]^+$) and (e) 4-unsaturated bond-containing PCs (PC 38:4 m/z = 848.5566 $[M + K]^+$ and PC 36:4 m/z = 820.5253 $[M + K]^+$) in control or *Acsl6*$^{-/-}$ cerebellum (Cere) or Striatum (Scale bars: 500 mm), $n = 1$. Data represent mean ± SEM; * by genotype within age, $p \leq 0.05$ by Student's *t*-test.

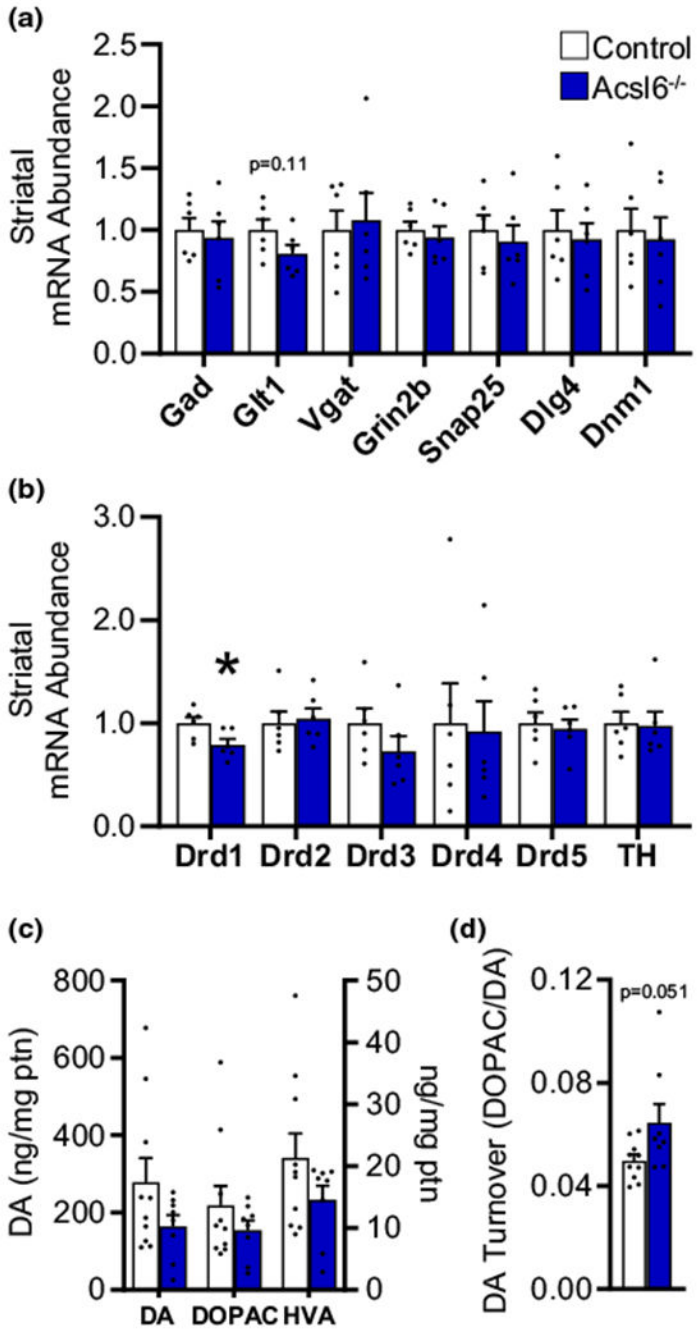

FIGURE 3.

ACSL6 loss influences dopamine metabolism. mRNA abundance of (a) glutamate metabolism and synaptic protein-related genes and (b) dopaminergic receptors and tyrosine hydroxylase genes in control and *Acsl6*$^{-/-}$ striatum, expressed relative to control mice, n = 6. (c) Abundance of dopamine and dopamine metabolites and (d) dopamine turnover rates in control and *Acsl6*$^{-/-}$ male mouse striatum, n = 8–10. Data represent mean ± SEM; * by genotype within age, $p \leq 0.05$ by Student's t-test.

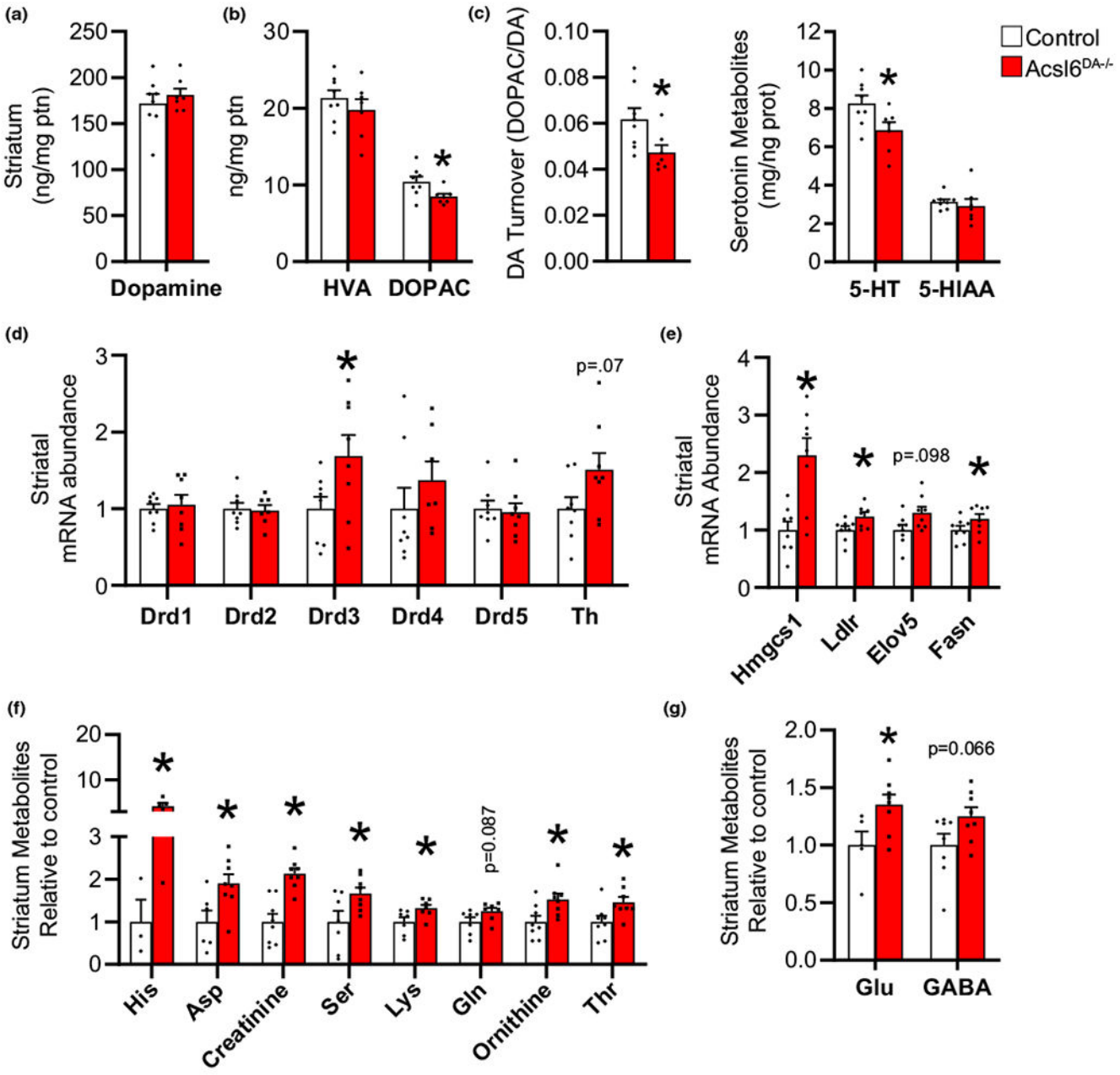

FIGURE 4.

Loss of ACSL6 specifically in dopaminergic neurons regulates striatal neurochemistry. (a) Abundance of dopamine, (b) dopamine metabolites, (c) dopamine turnover, and (d) serotonin and metabolites in male control and *Acsl6*$^{-/-}$ striatum, $n = 7–8$. mRNA abundance of (e) glutamate metabolism and (f) SREBP-responsive genes in control and *Acsl6*$^{-/-}$ striatum, expressed relative to control mice, $n = 7–8$. Striatal metabolite abundance for (g) amino acids and (h) GABA and glutamate in male control and *Acsl6*$^{-/-}$ striatum, expressed relative to control mice, $n = 3–8$. Data represent mean ± SEM; * by genotype within age, $p \leq 0.05$ by Student's *t*-test.

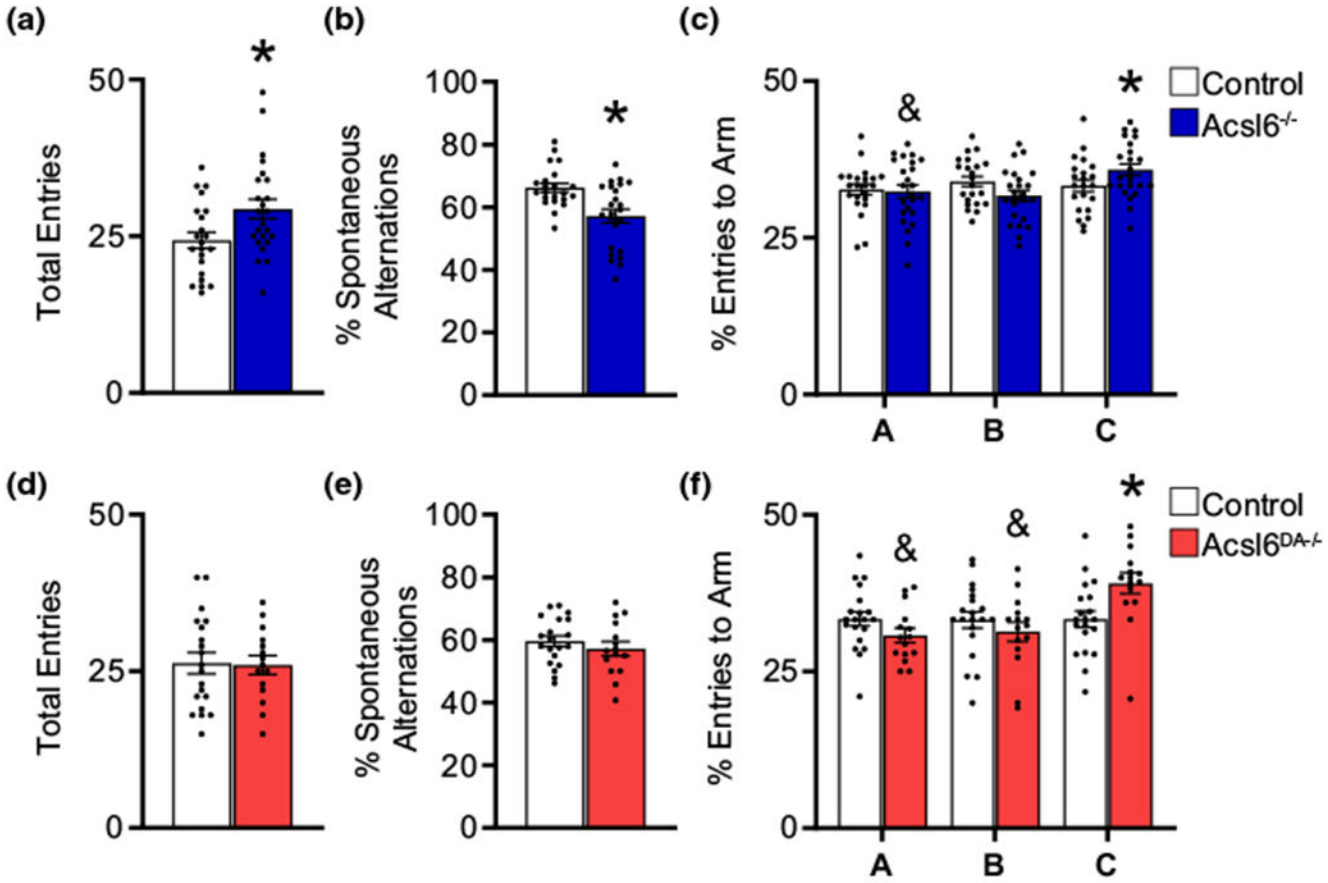

FIGURE 5.

Impaired response to Y-maze in germline ACSL6-deficient mice. Y-maze response for (a, d) total entries, (b, e) % spontaneous alternations, and (c, f) % entries by the arm of control, *Acsl6*$^{-/-}$ and *Acsl6*$^{DA-/-}$ male and female mice, $n = 15–20$. Data represent mean ± SEM; * by genotype within age, and compared to control entries for (c), $p \leq 0.05$ by Student's *t*-test. Data for *Acsl6*$^{-/-}$ were previously reported (Fernandez et al., 2021), shown here for comparison to *Acsl6*$^{DA-/-}$.

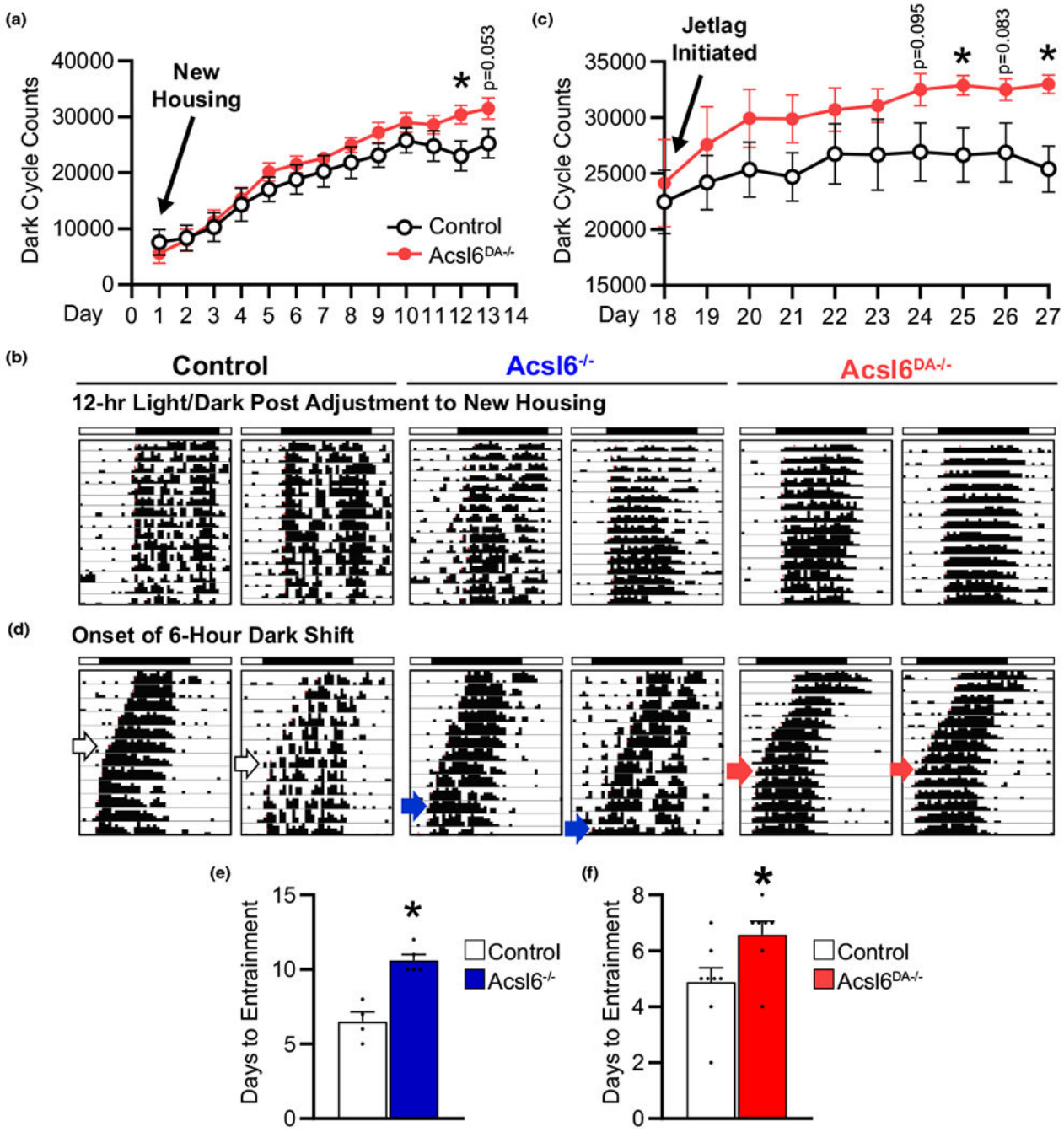

FIGURE 6.

Dopaminergic ACSL6 is required for recovery from photoperiod entrainment. Total wheel turns in the dark cycle during (a) adjustment to new housing and (c) adjustment after jetlag initiation of control and *Acsl6*$^{DA-/-}$ male mice, $n = 7–8$. Representative examples of wheel turn activity during the light and dark cycle (b) after adjustment to new housing or (d) upon jetlag initiation of control, *Acsl6*$^{-/-}$, and *Acsl6*$^{DA-/-}$ male mice, $n = 4–8$. Total number of days to entrainment post jetlag initiation in (e) *Acsl6*$^{-/-}$ or (f) *Acsl6*$^{DA-/-}$ male mice, and

respective control mice, $n = 4–8$. Data represent mean ± SEM; * by genotype comparison, $p \leq 0.05$ by Student's *t*-test.